https://doi.org/10.3311/PPci.37264 | 621
Creative Commons Attribution

Periodica Polytechnica Civil Engineering, 69(2), pp. 621–632, 2025

Stability Analysis of Slopes under Surcharge Loading Using FE Stress Deviator Increasing Method-proposal of Stability Charts

Lamia Medjitna[1], Amina Kahlerras[1], Djillali Amar Bouzid[1*]

[1] Laboratory of Numerical and Experimental Investigations in Geotechnical Engineering (NEIGE), Department of Civil Engineering, Faculty of Technology, University of Blida 1, P. O. B. 270, 09000 Blida, Algeria
[*] Corresponding author, e-mail: amarbouzid_djillali@univ-blida.dz

Received: 05 May 2024, Accepted: 24 January 2025, Published online: 27 February 2025

Abstract

Given the well-known shortcomings of the traditional limit equilibrium methods (LEMs) in addressing slope stability issues, there has been a growing interest towards employing finite element analysis as a viable alternative in recent years. However, due to the inherent limitations in the conventional finite element analysis, the application of finite element method (FEM) as a strength reduction method (SRM) or as finite element limit analysis (FELA) does not consistently yield successful results. To improve the efficiency of finite element analysis for addressing slope stability problems, a new methodology called 'Stress Deviator Increasing Method' (SDIM) has been recently proposed. It involves gradual expansion of the mobilized stress Mohr's circles until the soil failure takes place according to a predefined non-convergence criterion. In this paper an attempt is made to analyze the effects of surcharge loading on both factor of safety (FOS) value and location of the slip line using the finite element by SDIM by carrying out a restricted parametric study. Specifically, the effects of surcharge loading magnitude, the proximity of the surcharge with respect to the slope edge and the load distribution span were thoroughly analyzed and documented in the light of FOS values and plastic strain regions. The paper ends by proposing design stability charts in which, for a given surcharge magnitude and a geometric configuration, the user is able to determine the FOS for a combination of soil strength parameters.

Keywords

slope stability analysis, finite element analysis, limit equilibrium methods, stress deviator, surcharge loading, factor of safety

1 Introduction

Assessing the stability of slopes plays a vital role in geotechnical engineering projects, such as road embankments, dams, levees, highways, and structures built on slopes. An inaccurate evaluation of the safety factor can result in potentially catastrophic landslides, posing a severe risk to both structures and human lives.

For nearly a century, several methods have been developed for analyzing slope stability. Among the oldest, those of the limit equilibrium methods Bishop [1]; Lowe and Karafiath [2]; Morgenstern and Price [3]; Spencer [4]; Janbu [5]; Sarma [6]. It is important to note that these methods are based on simplifying assumptions and should be used with caution.

The finite element method (FEM) is widely used today for calculating slope stability problems. It is more rigorous and precise and does not require assumptions about interslice forces or the sliding surface. One of these methods, known as the soil strength reduction method (SRM) [7–15], involves reducing the shear strength parameters until a situation of failure is reached. Another approach, finite element limit analysis (FELA) [16–19], provides rigorous upper and lower bounds of the safety factor, although it is limited to problems where only an associated plasticity flow rule is allowed. A third finite element approach called 'stress deviator increasing method' (SDIM) Amar Bouzid [20, 21] has recently been developed to assess slope stability factor of safety by modifying the in-situ principal stresses while keeping the soil strength parameters unchanged. The SDIM is an innovative method which has the advantage of preserving the validity of the safety factor definition in the sense that the evolution of the mobilized shear stress corresponds to the same mobilized normal stress at every discretized point within the medium.

Cite this article as: Medjitna, L., Kahlerras, A., Amar Bouzid, D. "Stability Analysis of Slopes under Surcharge Loading Using FE Stress Deviator Increasing Method-proposal of Stability Charts", Periodica Polytechnica Civil Engineering, 69(2), pp. 621–632, 2025. https://doi.org/10.3311/PPci.37264

In many geotechnical situations, both artificial and natural slopes can experience external loads and surcharges stemming from the construction of nearby buildings or vehicle traffic in the case of roads. The presence of these loads may cause instability of the slope. In such a condition, the value of the safety coefficient depends on several parameters, including the geometric characteristics of the slope, the distance between the building foundation and the edge of the slope and the magnitude of the applied surcharge, among others.

The presence of a foundation generating an external surcharge on a slope is a complex issue that has been the subject of several studies. Pantelidis and Griffiths [22] demonstrated through a parametric study conducted within the framework of the limit states of EC7 that the type of failure mechanism of a foundation at the edge of a slope strongly depends on its size and position. Xie et al. [23] assessed the transition between the bearing capacity of a foundation and slope stability mechanisms based on the foundation location relative to the slope edge. The study, conducted through two failure mechanisms, revealed the relationship between the foundation setback distance and the failure mode of the foundation-slope system. By using the material point method (MPM), Xie et al. [24] analyzed the failure mechanism of the foundation-slope system and concluded that the setback distance of the load, the slope inclination angle, and soil strength parameters have a significant effect on the bearing capacity of the foundation.

These authors proposed a classification of failure modes of the foundation-slope system based on the foundation setback distance and defined the critical failure mode, which represents the transition between foundation failure and slope instability. Zhu et al. [25] analyzed the stability of a slope subjected to a localized overburden using a method based on the virtual distribution of multiple deformation lines. Baah-Frempong and Shukla [26] conducted a series of analyses, considering factors such as slope inclination, relative soil density, foundation distance from the slope edge, foundation depth, and the intensity of the load on a buried foundation at the slope crest using the SRM. They assessed the impact of these parameters on slope stability and subsequently proposed stability charts. Wang et al. [27] employed the variable-controlling method to evaluate slope stability, based on a horizontal distribution of deformations and the SRM analysis. The study, carried out under various loading conditions, showed that the deformation parameters can accurately reflect slope stability conditions. Zhang et al. [28] studied the stability and interaction mechanism of slope-pile-foundation systems under surcharge loading using the finite difference method. They analyzed in particular the effect of surcharge parameters, such as intensity, position, and width, on the failure modes of the slope, the evolution of the critical slip surface, as well as the stress and strain characteristics. The results showed that the surcharge parameters significantly affect the stability of the slope-pile-foundation system. Ishak et al. [29] investigated the behavior of a silica sand slope under surcharge loading using both limit equilibrium method (LEM) and finite element method (FEM). The authors carried out a consolidated drained (CD) triaxial test to determine the parameters of the silica sand. Experimental observation revealed that applying a surcharge to the slope crest resulted in deformation and swelling. The experimental results were validated by numerical models. Zhang et al. [30] employed the Material Point Method to assess the impact of surcharge loads on mixed soil-rock slopes and compared their response to that of pure soil slopes under similar loading conditions. The study quantified the distribution of plastic zones and morphological alterations of the slopes at characteristic stages. The comparative assessment revealed distinct damage patterns for different slope types, enhancing the understanding of their behavior under varying surcharge intensities.

The objective of this paper is to determine the parameters that influence the behavior of a slope subjected to a surcharge using the stress deviator increasing method (SDIM). The effect of the magnitude of the applied surcharge, its distance from the slope edge, and its distribution length are analyzed and the results are presented in terms of the safety factor. The slope failure mechanism and the distribution of deformations in the soil are also examined. Optimal values of surcharges and their locations on the slope can be deduced depending on the geometric and geotechnical parameters. Finally, slope stability charts established by the SDIM are proposed for different surcharge values. These charts can be used to quickly evaluate the slope safety factor as a function of the applied surcharge.

2 Short description of the FE procedure SDIM

The methodology utilized in this paper is termed the Stress Deviator Increasing Method (SDIM). It employs a finite element strategy where stress Mohr's circles, corresponding to the mobilized principal stresses, are systematically increased until a failure criterion is attained. This method, extensively discussed in works by Amar Bouzid [20, 21], aims to overcome the existing limitations in both the Limit Equilibrium Methods (LEMs) and the Strength Reduction Method (SRM) while offering various advantages. This paper presents a concise overview of the SDIM theory that has been implemented in a Fortran computer program named S[4]DINA 3.

In this approach, the process of computation involves incrementally raising a coefficient termed the "Mohr circle expansion coefficient" until the slope failure is reached. F^{Trial} is then used to control the rate of expansion of the Mohr circle. This coefficient is given by:

$$F^{Trial} = \frac{\tau^{Trial}}{\tau^{m}_{SDIM}} \quad (1)$$

The fundamental concept involves the expansion of the initial principal stresses of the Mohr's circle with the objective of maintaining the parallel orientation of the line $o_o i$ to the subsequent line of the Mohr's circle $o_t t$ (Fig. 1). This alignment ensures that both the mobilized shear stress τ^{m}_{SDIM} and the trial shear stress τ^{Trial}, occur on the same plane, thereby preserving the Factor of Safety (FOS) definition in terms of shear stresses.

The critical equations derived from the SDIM, are the expressions of principal stresses trial values. These equations have been developed to control the expansion of Mohr's circle in function of the increased value of F^{Trial}. The resulting trial principal stresses are as follows:

$$\sigma_1^{Trial} = \frac{s_0 + D_0 F^{Trial}(1+\sin\phi) - D_0 \sin\phi}{2} \quad (2)$$

$$\sigma_3^{Trial} = \frac{S_0 + D_0 F^{Trial}(\sin\phi - 1) - D_0 \sin\phi}{2} \quad (3)$$

Expressions 2 and 3 reduce to the following equations for purely cohesive soil:

$$\sigma_1^{Trial} = \frac{S_0 + D_0 F^{Trial}}{2} = \sigma_1^0 + \frac{D_0}{2}\left(F^{Trial} - 1\right) \quad (4)$$

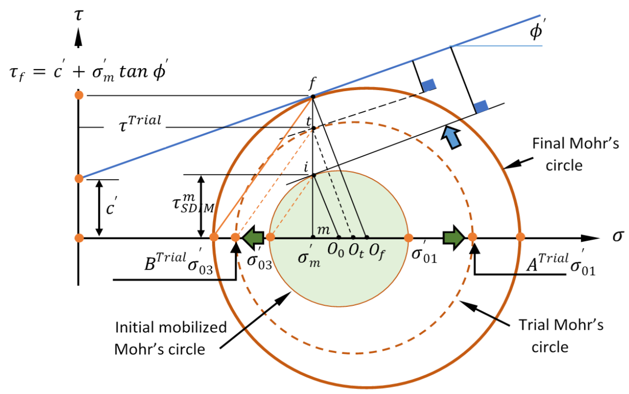

Fig. 1 Evolution of the mobilized stress Mohr's circle in the SDIM

$$\sigma_3^{Trial} = \frac{S_0 - D_0 F^{Trial}}{2} = \sigma_3^0 - \frac{D_0}{2}\left(F^{Trial} - 1\right) \quad (5)$$

Where, S_0 is mobilized principal stress sum, D_0 is the mobilized principal stress deviator and ϕ is the internal friction angle.

As the expansion factor F^{Trial} is gradually raised, stress points with trial stresses reaching their ultimate values undergo plastic deformation and generate plastic zones that continue to spread. At this point, F^{Trial} is assumed to have reached the stress point-based factor of safety, denoted as FOS^{SP}_{SDIM} which is calculated using the following formula:

$$FOS^{sp}_{SDIM} = \frac{\tau^{f}_{SDIM}}{\tau^{m}_{SDIM}} \quad (6)$$

From Fig. 1, the analytical evaluation of FOS^{SP}_{SDIM} is:

$$FOS^{sp}_{SDIM} = \frac{2c}{D_0\cos\phi} + \tan^2\phi\left(\frac{S_0}{D_0\sin\phi} - 1\right) \quad (7)$$

For a purely cohesive soil, the analytical expression of FOS^{SP}_{SDIM} is:

$$FOS^{sp}_{SDIM} = \frac{2c}{D_0} \quad (8)$$

The overall FOS, is not attained as long as the solution of the algebraic system of equations is still converging. However, when the whole system fails to converge by reaching the maximum number of iterations according to a convergence criterion, the last value of F^{Trial} is assumed to be the overall FOS. Therefore, the accuracy of FOS depends obviously on the accuracy of FOS^{SP}_{SDIM} .

3 Effect of external loading on the Slope stability using the SDIM-A parametric analysis

In practical situations, it is common to encounter external loads at the edge of a slope, such as those associated with building foundations, bridge abutments, or road loads acting on an underlying embankment.

When the soil at the top of the slope is subjected to loading, shear strength increases, leading to an increase in shear stresses. Soil failure then depends on various variables such as soil strength parameters, slope inclination, the length of load distribution, and its position relative to the slope edge. Optimal values can be determined through a stability analysis.

In the following, the stability of a slope under the influence of an overburden is assessed through a parametric analysis. Stability is evaluated in relation to the slope inclination, the magnitude of the load and its positioning relative to the slope edge.

3.1 Effect of the slope inclination angle

To assess the effect of varying the inclination angle on stability, the slope shown on Fig. 2 is considered.

The soil deposit has an effective cohesion c = 20 kPa, an effective friction angle ϕ = 20°, and a unit weight γ = 20 kN/m^3. A surcharge of ($q/\gamma H$ = 0.5) over a span of B = 2.5 m, is placed at a distance of b = 1 m from the edge of the slope. The slope stability factor is computed for four distinct slope inclinations β = 30°, 45°, 60° and 90°. When LEMs are involved for comparison purposes, the software SLIDE 6.0 software [31] is employed.

The results of the variation in the safety factor as a function of the slope inclination obtained with SDIM were compared with those from the simplified Bishop method [1] and the Spencer method [4] included in SLIDE 6.0 and are presented in the Table 1.

As expected, when the inclination increases, slope instability increases, and the safety factor decreases. The curve obtained by SDIM in Fig. 3 is nearly identical to those obtained by both Bishop and Spencer methods, with a slight deviation in the safety factor for β = 90°.

Fig. 4 shows the distribution of the equivalent plastic strain $\bar{\varepsilon}_v$ for different slope inclinations. It is evident that changing the slope inclination under a fixed surcharge directly affects its stability. For low inclinations (β = 30°) with a safety factor F_{SDIM} = 1.35, plastic deformations are distributed vertically and directly beneath the surcharge, indicating a soil bearing capacity rather than a slope stability problem. This fact is in accordance with the results of Wang et al. [27]. For a moderate slope (β = 45°), the safety

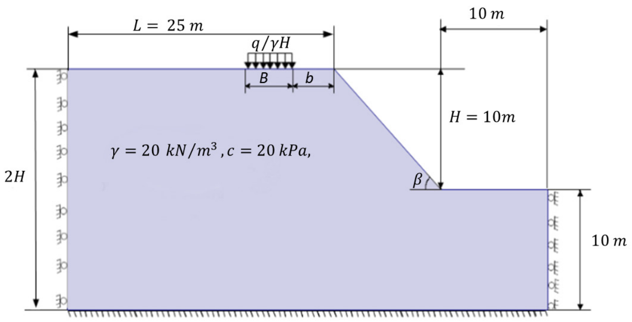

Fig. 2 Geometry and characteristics of the soil slope

Table 1 FOS values obtained by different methods for $q/\gamma H$ = 0.5

β	S^{4}DINA 3.0	SLIDE 6.0 [4]	SLIDE 6.0 [1]
30°	1.35	1.36	1.37
45°	0.96	1.00	1.01
60°	0.78	0.79	0.8
90°	0.55	0.5	0.46

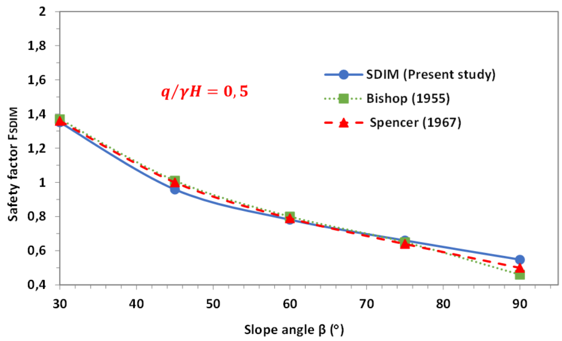

Fig. 3 Safety factor as a function of the slope inclination angle

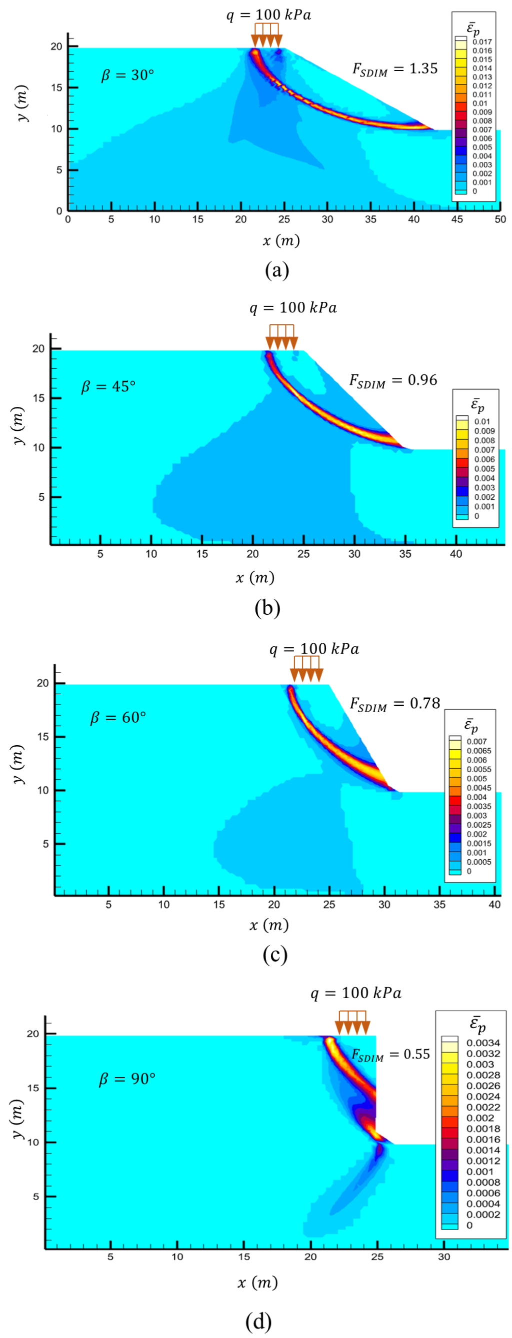

Fig. 4 Effect of slope angle on contour lines at failure: (a) β = 30°, (b) β = 45°, (c) β = 60°, (d) β = 90°

factor F_{SDIM} = 0.96 and the area of plastic deformations is less pronounced towards the slope bottom.

However, further plastic areas appear near the slope surface, indicating an instability mechanism. In the case of a vertical slope (β = 90°), two slip lines exhibit distinct failure mechanisms. The initial starts from the slope crest and extends the mid-slope height, whereas the second initiates at the slope toe and progresses downwards towards the slope base.

3.2 Effect of surcharge load magnitude

The effect of varying the overburden on slope stability is analysed by applying progressively increasing loads ranging from 25 to 300 kPa ($q/\gamma H$ between 0.125 and 1.5), and positioned at a fixed distance of 1 m from the slope's edge for a slope inclination of β = 45°.

The evolution of factor of safety provided by SDIM and those of LEMs in terms of $q/\gamma H$ is illustrated in Fig. 5.

Firstly, the variation curve of the safety factor as a function of the relative overburden obtained by SDIM is compared with those obtained by the simplified Bishop and Spencer methods. The safety factor values obtained by SDIM are slightly lower than those obtained by the slice method, which can be explained by the use of a non-associated flow rule in the SDIM [21]. The curves exhibit the same trend, which is a decrease in the safety factor with an increase in the surcharge.

The Figs. 6 (a)-(d) display the distribution of $\bar{\varepsilon}_p$ contour lines and the failure mode of a slope subjected to increasing overburden. As expected, the slope failure mechanism strongly depends on the magnitude of the applied load Zhu et al. [25]. Indeed, for loads of low to moderate intensity ($q/\gamma H$ less than 0.5), the failure surface is well-defined, and the slope exhibits a deep failure reaching the toe of the slope (toe failure surface). As the overburden increases, the depth of the failure slip line decreases, giving birth to a mechanism resembling that of a shallow foundation bearing capacity mechanism Pantelidis and Griffiths [22]. For heavy loads, the slope failure is localized at the slope inclined face.

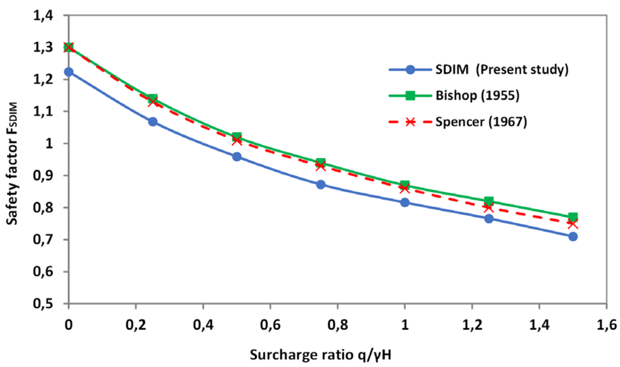

Fig. 5 Safety factor as a function of the relative surcharge $q/\gamma H$

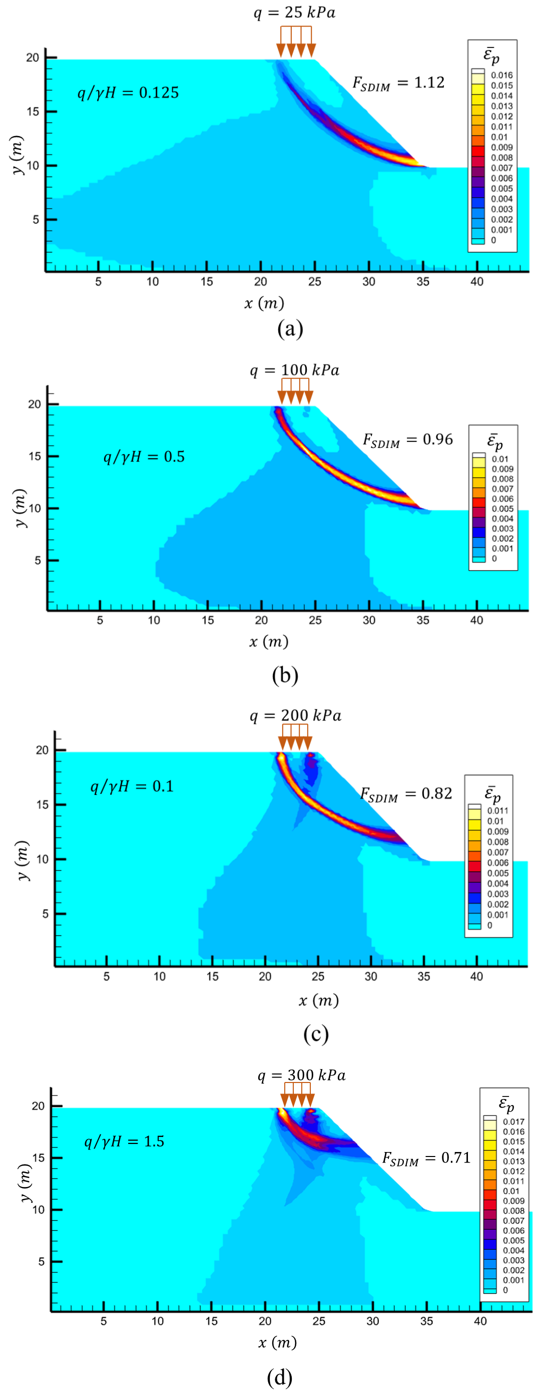

Fig. 6 Effect of surcharge load on $\bar{\varepsilon}_p$ contour lines at failure: (a) $q/\gamma H$ = 0.125 , (b) $q/\gamma H$ = 0.5, (c) $q/\gamma H$ = 0.1, (d) $q/\gamma H$ = 1.5

3.3 Effect of the proximity of the surcharge load to the slope edge

Several studies have analysed the effect of varying the proximity of an overburden to the edge of a slope to determine the critical setback distance from which the load no longer affects the slope's stability. In this context, an overburden q = 100 kPa is placed at the top of a slope with a fixed height H = 10 m. The parametric analysis pertains to the influence of varying relative setback distance ratios of b/B = 0.0, 2.0, 3.0, 4.0 and 6.0 on the slope factor of safety.

In order to assess both the influence of the slope inclination and the setback distance ratio on the slope stability factor, four different inclinations β = 30°, 45°, 60° and 75° were considered. The resulting curves are shown of the Fig. 7. Upon initial observation, it is apparent that these curves illustrate an identical pattern, characterized by a linear segment between b/B = 0.0 and b/B = 3.5. Subsequently, there is an approximate horizontal line, indicating a marginal impact of the setback distance on the F_{SDIM} regardless the value of slope inclination β. An optimal setback for which the external loading has no influence on the F_{SDIM} can be set as b/B = 3.5.

Fig. 8 illustrates the distribution of the equivalent plastic strain $\bar{\varepsilon}_p$ contour lines at failure along with the value of factor of safety for different loading placements.

The initial observation is evident: as the distance between the load and the edge increases, its impact on slope stability diminishes, leading to an increase in the safety factor (Figs. 8 (b)-(f)).

Specifically, the safety factor rises as the relative distance grows and stops when b/B reaches a critical value of approximately 3.5. Beyond this critical distance, the presence of the load ceases to affect the stability, and the slope stability factor in nearly identical to the same slope without external loading. For a slope without overburden (Fig. 8 (a)), the failure slip line appears at the toe of the slope, and the safety factor is F_{SDIM} = 1.70. When an external loading of magnitude equal to 100 kPa is placed at slope edge (Fig. 8(b)), the FOS becomes unstable with a F_{SDIM} = 1.35. In this case, plastic deformations primarily concentrate under the load and near the slope surface.

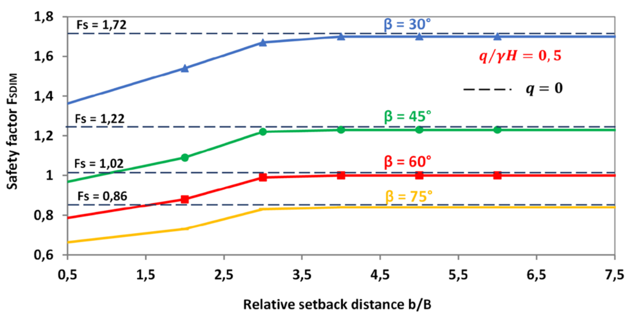

Fig. 7 Variation of the safety factor (F_{SDIM}) as a function of the setback distance b/B for different slope angles

As the load moves away from the edge, the safety factor increases to attain 1.54 (Fig. 8 (c)) and 1.67 (Fig. 8 (d)) for respectively b/B = 2.0 and b/B = 3.0. Beyond a critical setback distance, evaluated as b/B = 3.5, the slope behaviour at failure reveals two distinct failure mechanisms (Figs. 8 (e) and (f)). The first which occurs in the sloping ground and slipe line is similar to that of a slope without surcharge loading. In these conditions, the stability becomes completely independent of the influence of the load and the safety factor recovers its initial value of F_{SDIM} = 1.70.

Figs. 9 (a)-(f) illustrate the distribution of the equivalent plastic strain $\bar{\varepsilon}_p$ contour lines at failure along with the value of factor of safety for different loading placements for a slope with an inclination angle β = 75°.

The second failure mechanism occurs directly beneath the load, indicating a shallow foundation bearing capacity issue.

The same observations can be made regarding the variation of the safety factor and the distribution of plastic deformations. In fact, the safety factor is F_{SDIM} = 0.84, for a slope of β = 75° without surcharge (Fig. 9 (a)). In the presence of a surcharge of q = 100 kPa on the edge, it drops to F_{SDIM} = 0.66 (Fig. 9 (b)). The safety factor then increases gradually as the load moves away from the edge (Figs. 9 (c)-(d)) to reach the previous value of a slope without surcharge of F_{SDIM} = 0.84 for a relative setback distance of b/B = 4. The distribution of equivalent plastic deformations is practically identical to that of the slope of β = 30°, without surcharge. The closer the surcharge is to the edge, the more the plastic zones concentrate near the slope, indicating its instability.

3.4 Influence of the load distribution length

To analyse the effect of the load distribution length B on the stability of a slope, the safety factor is evaluated for a slope subjected to a surcharge loading of q = 100 kPa distributed over a length B ranging from 2.50 to 20.0 m. The slope has a height H = 10 m and has a variety of inclination angles β. Fig. 10 shows the variation of the safety factor F_{SDIM} with the relative distribution length of the surcharge B/L for slope angles β varying from 30° to 90°.

The first observation is that the curves have the same trend regardless of the slope angle. The second observation is that the safety factor decreases slightly when the distribution length B/L increases from 0.1 to 0.2, then stabilizes for $B/L > 0.2$. Based on these results, it can be concluded that increasing the distribution length of the surcharge has no significant effect on slope safety beyond a relative distance of 0.2.

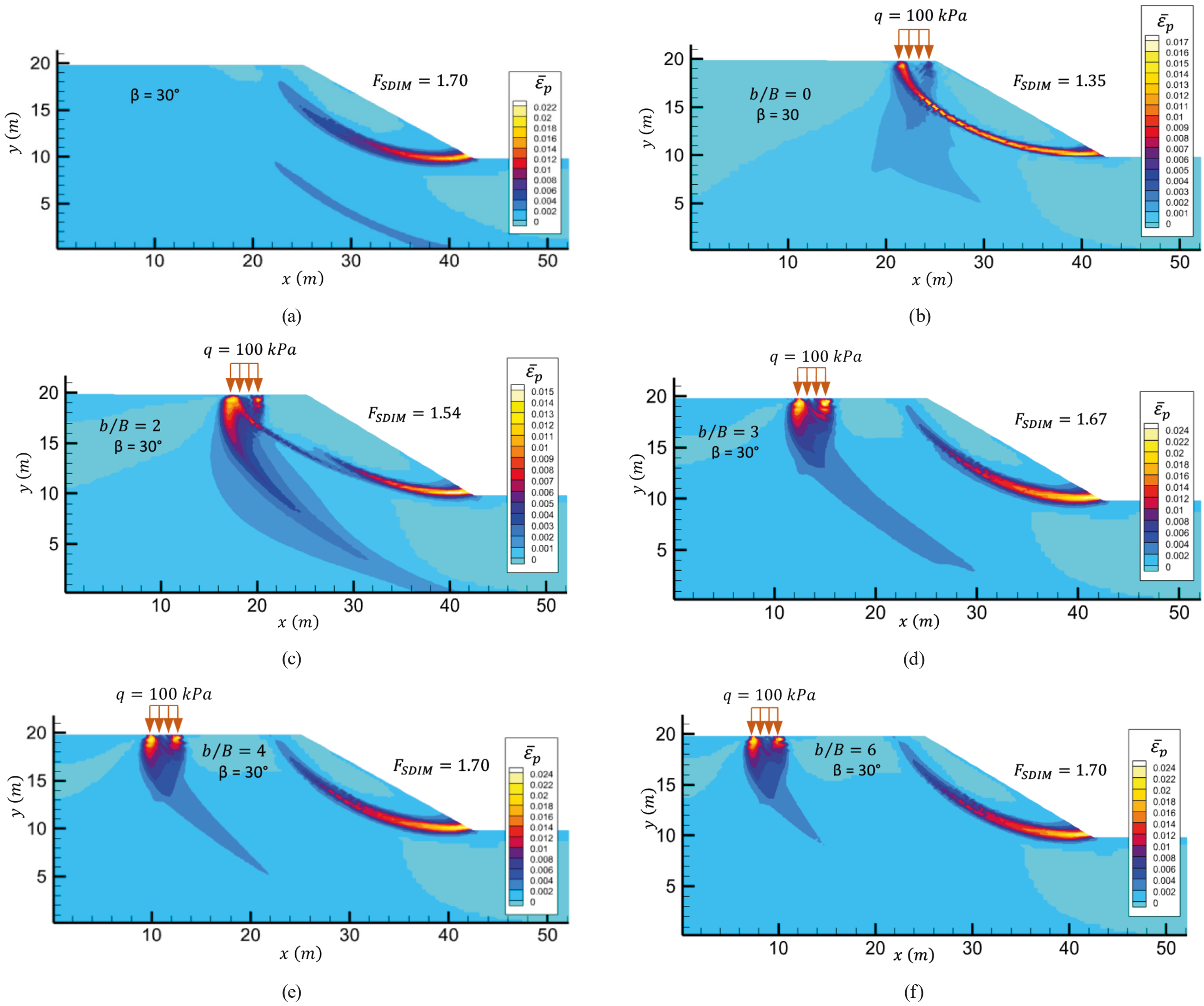

Fig. 8 Effect of loading position on $\bar{\varepsilon}_p$ contour lines at failure: (a) $q = 0$, (b) $b/B = 0$, (c) $b/B = 2$, (d) $b/B = 3$, (e) $b/B = 4$, (f) $b/B = 6$

Figs. 11 (a)-(d) illustrate $\bar{\varepsilon}_p$ contour lines at failure as well as the safety factor as a function of the load distribution length for a slope angle of $\beta = 45°$. The slope stability is minimally affected by the variation in the distribution length. In fact, the safety factor slightly decreases from 0.96 to 0.93 as B/L varies from 0.1 to 0.4, and then stabilizes at $B/L = 0.8$.

This confirms that increasing the load distribution distance has practically no effect on the value of slope stability factor.

Although the F_{SDIM} is not affected, the load distribution span notably impacts the $\bar{\varepsilon}_p$ contour lines at failure. In fact, when the relative distance is small ($B/L = 0.1$), the slip line is well defined and the zone beneath the surcharge load remains elastic.

However, when B/L increases, the soil beneath the right edge of the surcharge loading becomes more overstrained giving birth to a second slip line. The plastic deformations spread towards the left boundaries of the discretized model.

4 Stability charts proposal

Stability charts have been devised to facilitate a rapid initial assessment of the safety factor. Several authors in the past proposed charts for safety factor determination. Among these pioneers, Taylor [32] introduced stability charts for slope stability using the ϕ-circle method and defined the stability number N in function of the stability factor F as $c/\gamma HF$ to present the results in dimensionless form. Nonetheless, Taylor's charts have some drawbacks, as they do not provide any indication of the location of the failure circle, and the definition of the safety factor necessitates an iterative computation. Over the years, numerous suggestions based on limit equilibrium methods (LEMs) or finite element limit analysis (FELA) have been made to enhance Taylor's charts and eliminate the need for an iterative process. Michalowski [33] produced a series of stability charts based on finite element limit analysis, offering non-iterative

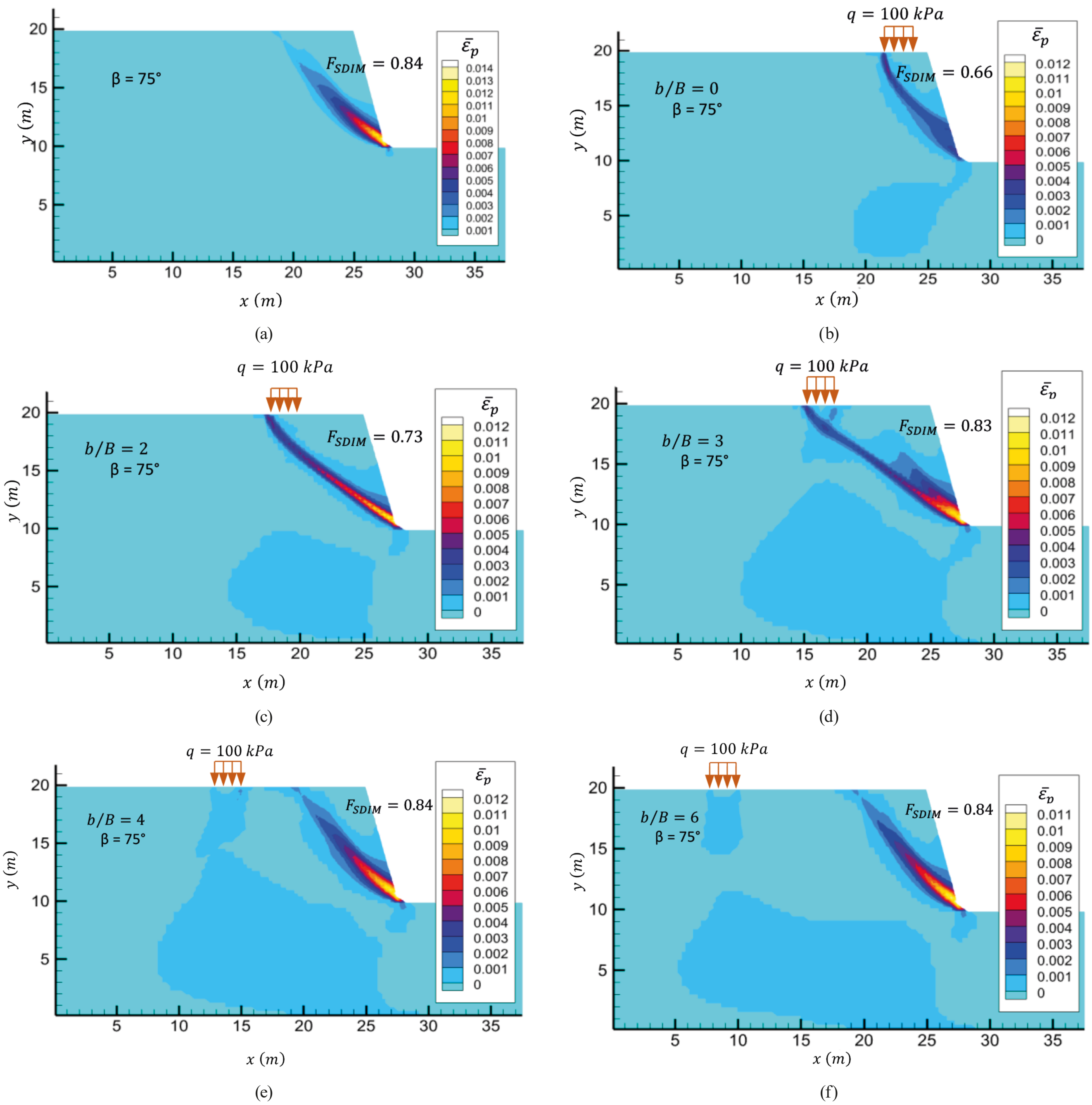

Fig. 9 Effect of loading position on $\bar{\varepsilon}_p$ contour lines at failure: (a) $q = 0$, (b) $b/B = 0$, (c) $b/B = 2$, (d) $b/B = 3$, (e) $b/B = 4$, (f) $b/B = 6$

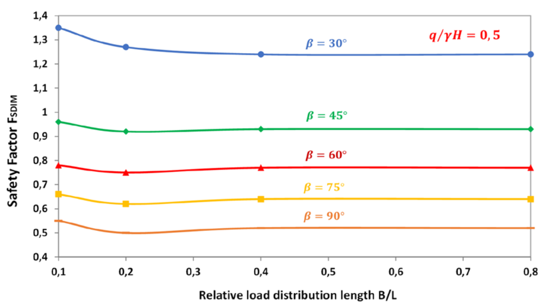

Fig. 10 Variation of the safety factor (F_{SDIM}) as a function of the loading span B/L for different slope angles

calculation process. The proposed charts are suitable for slopes subjected to water pore pressure and seismic forces. The effect of water pore pressure was also considered by Sun and Zhao [34] in stability charts based on limit equilibrium methods. Tang et al. [35] developed stability charts for homogeneous and isotropic slopes using the upper bound analysis theory and the strength reduction method. These charts accommodate various slope conditions, such as the presence of an external surcharge on the slope crest, water pore pressure, and horizontal seismic forces.

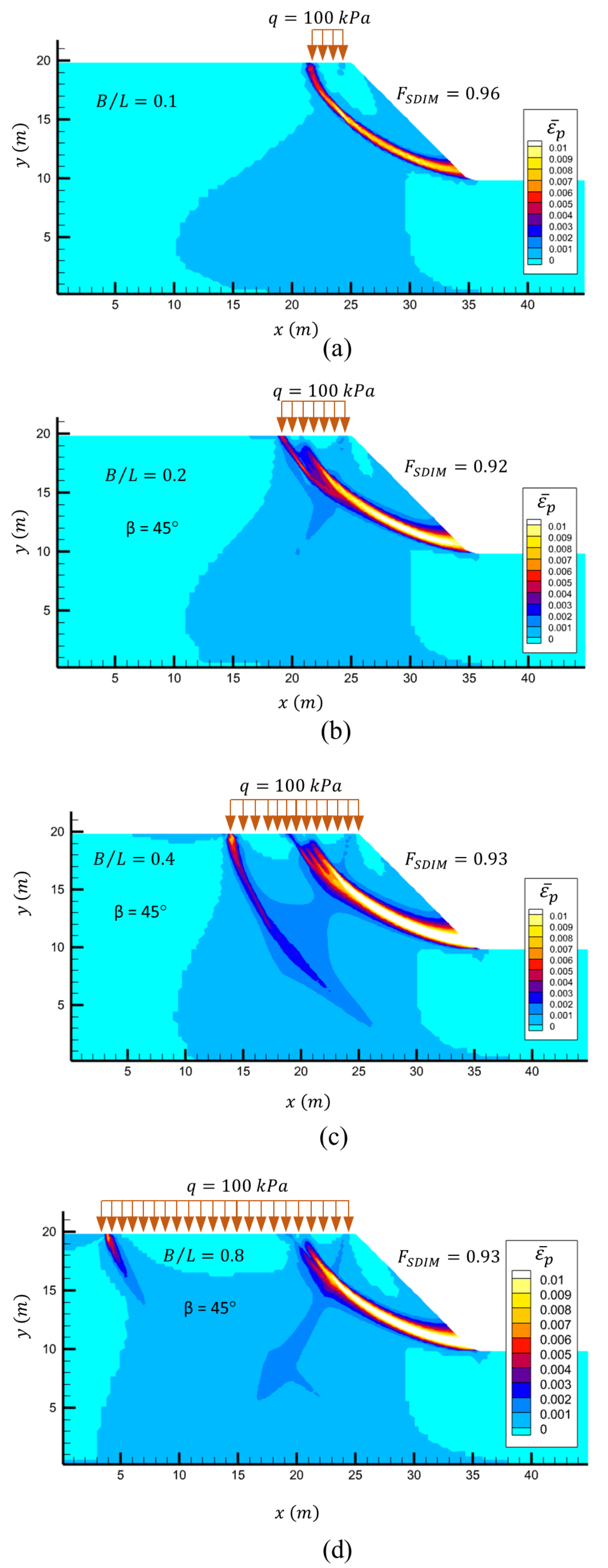

Fig. 11 Effect of loading span on $\bar{\varepsilon}_p$ contour lines at failure for $\beta = 45°$: (a) $B/L = 0.1$, (b) $B/L = 0.2$, (c) $B/L = 0.4$, (d) $B/L = 0.8$

In the following, the finite element procedure (SDIM) is employed to establish stability charts for a homogeneous slope subjected to a uniform surcharge load q at the slope crest. The slope geometric dimensions and surcharge distance and location are those previously presented in the Fig. 2. The charts have been developed for a slope inclination angle β ranging from 15° to 90°, and the surcharge is represented by the previously defined surcharge ratio $q/\gamma H$. Six surcharge ratios, namely: 0.0, 0.1, 0.2, 0.3, 0.4 and 0.5 were considered in the analysis. These charts for $q/\gamma H = 0.0$ through $q/\gamma H = 0.5$ are respectively illustrated by Figs. 12–17.

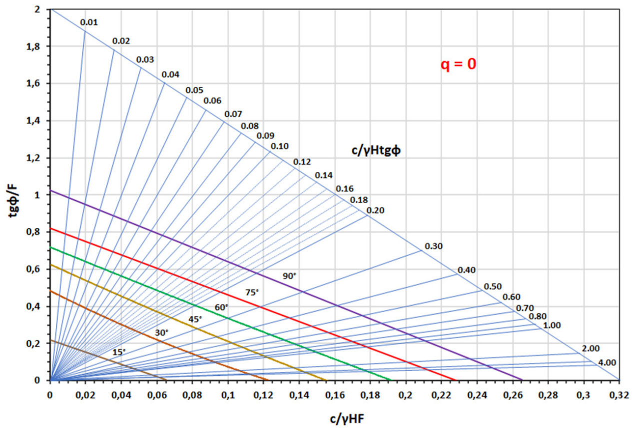

Fig. 12 Stability chart for homogeneous slope without surcharge

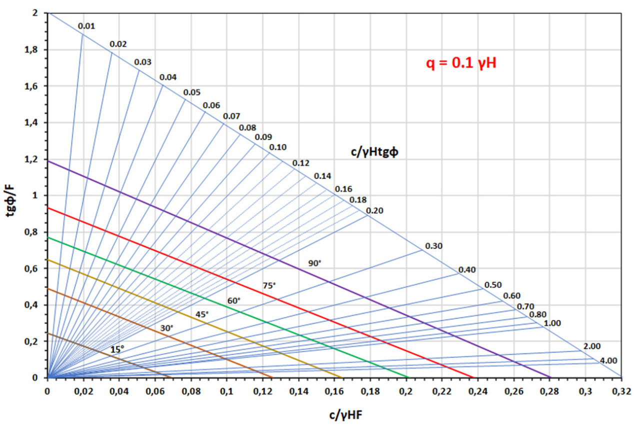

Fig. 13 Stability chart for homogeneous slope with surcharge load $q = 0.1\ \gamma H$

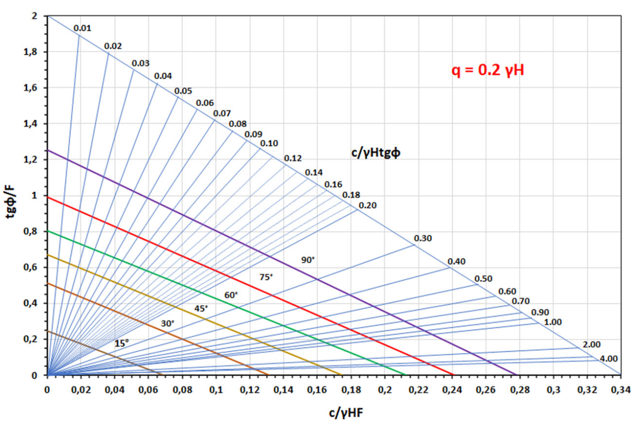

Fig. 14 Stability chart for homogeneous slope with surcharge load $q = 0.2\ \gamma H$

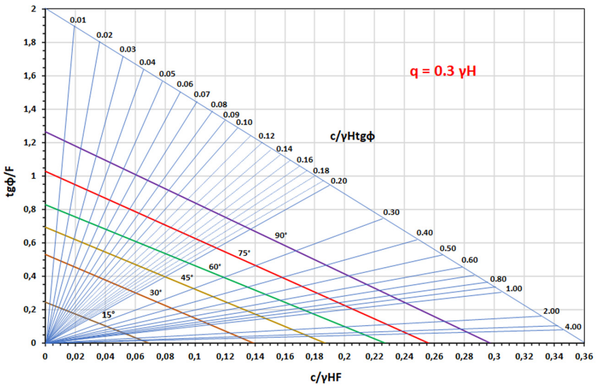

Fig. 15 Stability chart for homogeneous slope with surcharge load $q = 0.3\ \gamma$H

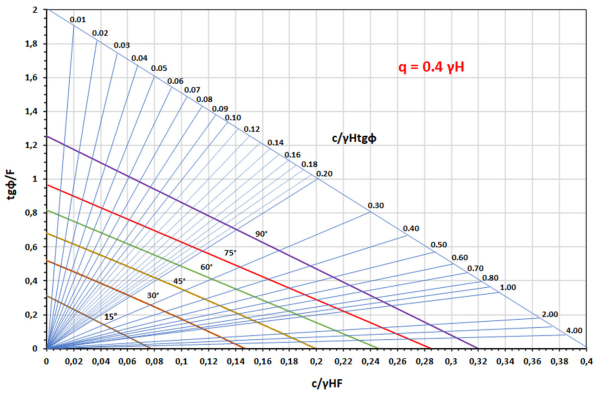

Fig. 16 Stability chart for homogeneous slope with surcharge load $q = 0.4\ \gamma$H

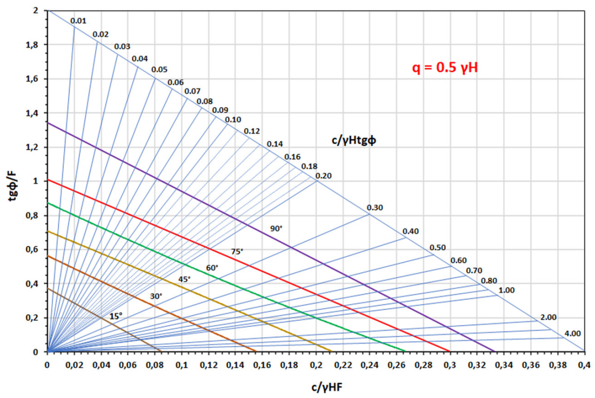

Fig. 17 Stability chart for homogeneous slope with surcharge load $q = 0.5\ \gamma$H

4.1 Calculation examples

The first example consists in homogeneous slope without any external surcharge having a height of H = 15 m, an inclination angle of β = 75° and soil strength parameters are: ϕ = 25°, c = 15 kPa, γ = 20 kN/m^3. The determination of the factor of safety requires the use of charts of Fig. 12. The necessary parameters and the FOS values obtained by the methods involved in the comparison, are gathered in Table 2.

The second example consists of a homogeneous slope subjected to an external surcharge ratio $q/\gamma H$ = 0.2. The slope has a height of H = 10 m, an inclination angle of β = 45° and soil strength parameters are: ϕ = 15°, c = 10 kPa, γ = 20 kN/m^3. Based on this information, the determination of the factor of safety requires the use of charts of Fig. 14. The necessary parameters and the FOS values obtained by the methods involved in the comparison, are reported in Table 3.

Tables 2 and 3 compare the safety factor values obtained from chart assessment for the two examples with those derived from the limit equilibrium (LE) and limit analysis (FELA) methods. The factors of safety (FOS) obtained through the Limit Equilibrium Method (LEM) were provided by SLIDE 6.0 using Spencer's approach, while those from Finite Element Limit Analysis (FELA) were obtained using the software OPTUM^{G2} [36]. The close agreement between the FOSs resulting from graphical assessment and those from finite element limit analysis strongly suggests that the charts generated by the SDIM method are reliable.

Therefore, they can be considered as a rapid alternative for accurately estimating the FOS for any combination of strength parameters.

Table 2 FOS values from graphical assessment and other methods for the example 1

Parameters	β(°)	$q/\gamma H$	$c/\gamma H\tan\phi$	$c/\gamma HF$	$\tan\phi/F$
Values	75.0	0.0	0.107	0.05	0.45
Factor of safety provided by:	Graphical assessment from charts of Fig. 12			0.77 or 0.79	
	SLIDE 6.0 (Spencer's method)			0.9	
	FELA (OPTUM^{G2})		Lower bound	0.76	
			Upper bound	0.77	

Table 3 FOS values from graphical assessment and other methods for the example 2

Parameters	β(°)	$q/\gamma H$	$c/\gamma H\tan\phi$	$c/\gamma HF$	$\tan\phi/F$
Values	45.0	0.2	0.19	0.074	0.39
Factor of safety provided by:	Graphical assessment from charts of Fig. 14			0.69 or 0.67	
	SLIDE 6.0 (Spencer's method)			0.7	
	FELA (OPTUM^{G2})		Lower bound	0.69	
			Upper bound	0.71	

5 Conclusions

A new finite element procedure called SDIM was recently proposed for the assessment of slope stability factor. The performances of this numerical procedure were confirmed when compared to other numerical approaches especially the finite element limit analysis (FELA). By systematically expanding Mohr's stress circle, the factor of safety is reached when the slope failure occurs, thus taking the reverse path of the SRM which consists of reducing the soil strength parameters. The slope failure is considered to take place when the iterative process fails to converge within a prescribed range of maximum number of iterations. In many geotechnical situations, both man-made and natural slopes can experience external loads and additional surcharges stemming from the construction of neighbouring buildings or vehicle movement in the case of roads.

The presence of these loads has a significant impact on the value of safety factor, potentially transforming the situation from a stability concern to a bearing capacity problem or a combination of both.

Consequently, other parameters such as surcharge intensity, the geometric distribution of the surcharge and the distance between the building foundation and the slope edge play a significant role in shaping the factor of safety, as well as determining the geometric configuration and position of the failure surface.

In order to quantify the effects of external surcharges applied on a slope, this paper attempts to analyse the effects of surcharge loading on both factor of safety and location of the slip line using the finite element by SDIM.

After a brief description of the SDIM approach, a parametric study was carried out. Specifically, the effects of surcharge loading magnitude, the proximity of the surcharge with respect to the slope edge and the load distribution span were thoroughly analysed and documented in the light of FOS values and plastic strain regions. The major conclusions reached are:

- For a given slope angle, the FOS decreases as the surcharge magnitude increases. Small to moderate surcharges lead to well defined failure surfaces characterized as toe-type. However, when the surcharge grows, slope face-type slip lines appear accompanied by the formation of a shallow foundation bearing mechanism immediately beneath the surcharge location.
- The effect of the surcharge setback distance is confined to a limited area near the slope edge defined as $b/B = 3.5$, regardless the slope inclination angle. When the ratio b/B is below 3.5, the failure surface undergoes disturbance, extending from the slope toe to the left end of the surcharge. Beyond this characteristic distance, the effect disappears and the slope FOS becomes equal to that of a surcharge-free slope. However, two distinct failure mechanisms occur in slope domain. A slip line identical to that of a slope without surcharge appears on the slope face, while a different failure mechanism, resembling a shallow foundation bearing mechanism initiates directly beneath the surcharge application span.
- The increasing of the surcharge distribution distance has only a marginal effect on the slope stability factor (FOS). Nevertheless, when the ratio B/L exceeds 0.2, another slip line appears beneath the left end of the distributed surcharge. The latter becomes less pronounced as the surcharge draws closer to the slope left boundary.

The paper concludes by suggesting design stability charts that enable users to determine the factor of safety (FOS) for various combinations of soil strength parameters, considering a given surcharge magnitude and a geometric configuration.

References

[1] Bishop, A. W. "The use of the slip circle in the stability analysis of slopes", Géotechnique, 5(1), pp. 7–17, 1955. https://doi.org/10.1680/geot.1955.5.1.7

[2] Lowe, J., Karafiath, L. "Stability of earth dams upon drawdown", In: Proceedings of the First Panamerican Conference on Soil Mechanics and Foundation Engineering, Mexico City, Mexico, 1992, pp. 537–552.

[3] Morgenstern, N. R., Price, V. E. "The analysis of the stability of general slip surfaces", Géotechnique, 15(1), pp. 79–93, 1965. https://doi.org/10.1680/geot.1965.15.1.79

[4] Spencer, E. "A method of analysis of the stability of embankments assuming parallel interslice forces", Géotechnique, 17(1), pp. 11–26, 1967. https://doi.org/10.1680/geot.1967.17.1.11

[5] Janbu, N. "Slope stability computations", Soil Mechanics and Foundation Engineering Report, The Technical University of Norway, Trondheim, Norway, 1968.

[6] Sarma, S. K. "Stability analysis of embankments and slopes", Géotechnique, 23(4), pp. 423–433, 1973. https://doi.org/10.1680/geot.1973.23.3.423

[7] Zienkiewicz, O. C., Humpheson, C., Lewis, R. W. "Associated and non-associated viscoplasticity and plasticity in soil mechanics", Géotechnique, 25(4), pp. 671–689, 1975. https://doi.org/10.1680/geot.1975.25.4.671

[8] Naylor, D. J. "Finite elements and slope stability", In: Martins, J. B. (ed.) Numerical Methods in Geomechanics, Springer Dordrecht, 1981, pp. 229–244. ISBN: 978-90-277-1461-9 https://doi.org/10.1007/978-94-009-7895-9_10

[9] Donald, I. B., Giam, S. K. "Application of the nodal displacement method to slope stability analysis", In: Proceedings of the 5th Australia-New Zealand Conference on Geomechanics, Sydney, 1988, pp. 456–460. ISBN: 0858254085

[10] Matsui, T., San, K.-C. "Finite Element Slope Stability Analysis by Shear Strength Reduction Technique", Soils and Foundations, 32(1), pp. 59–70, 1992. https://doi.org/10.3208/sandf1972.32.59

[11] Ugai, K., Leshchinsky, D. "Three-Dimensional Limit Equilibrium and Finite Element Analyses: A Comparison of Results", Soils and Foundations, 35(4), pp. 1–7, 1995. https://doi.org/10.3208/sandf.35.4_1

[12] Dawson, E. M., Roth, H., Drescher, A. "Slope stability analysis by strength reduction", Géotechnique, 49(6), pp. 835–840, 1999.

[13] Griffiths, D. V., Lane, P. A. "Slope stability analysis by finite elements", Géotechnique 49(3), pp. 387–403, 1999. https://doi.org/10.1680/geot.1999.49.3.387

[14] Cheng, Y. M., Lau, C. K. "Slope stability analysis and stabilization: New methods and insight", CRC Press, 2014. ISBN: 9780429166457 https://doi.org/10.1201/b17015

[15] Liu, S. Y., Shao, L. T., Li, H. J. "Slope stability analysis using the limit equilibrium method and two finite element methods", Computers and Geotechnics, 63, pp. 291–298, 2015. https://doi.org/10.1016/j.compgeo.2014.10.008

[16] Sloan, S. W. "51st Rankine lecture: geotechnical stability analysis", Géotechnique, 63(7), pp. 531–572, 2013. https://doi.org/10.1680/geot.12.RL.001

[17] Krabbenhoft, K., Lyamin, A. V., Sloan, S. W. "Formulation and solution of some plasticity problems as conic problems", International Journal of Solids and Structures, 44(5), pp. 1533–1549, 2007. https://doi.org/10.1016/j.ijsolstr.2006.06.036

[18] Tschuchnigg, F., Schweiger, H. F., Sloan, S. W. "Slope stability analysis by means of finite element limit analysis and finite element strength reduction techniques. Part I: numerical studies considering non-associated plasticity", Computers and Geotechnics, 70, pp. 169–177, 2015. https://doi.org/10.1016/j.compgeo.2015.06.018

[19] Tschuchnigg, F., Schweiger, H. F., Sloan, S. W., Lyamin, A. V., Raissakis, I. "Comparison of finite finite-element limit analysis and strength reduction techniques", Géotechnique, 65(4), pp. 249–257, 2015. https://doi.org/10.1680/geot.14.P.022

[20] Amar Bouzid, D. "Finite element analysis of a slope stability by incrementally increasing the mobilized principal stress deviator", Geomechanics and Geoengineering, 17(5), pp. 1554–1574, 2021. https://doi.org/10.1080/17486025.2021.1955157

[21] Amar Bouzid, D. "Finite element analysis of slope stability by expanding the mobilized principal stress Mohr's circles – Development, encoding and validation", Journal of Rock Mechanics and Geotechnical Engineering, 14(4), pp. 1165–1179, 2022. https://doi.org/10.1016/j.jrmge.2022.01.016

[22] Pantelidis, L., Griffiths, D. V. "Footing on the crest of slope: Slope stability or bearing capacity?", In: Engineering Geology for Society and Territory - Volume 2: Landslide Processes, Springer International Publishing, 2015, pp. 1231–1234. https://doi.org/10.1007/978-3-319-09057-3_215

[23] Xie, T. C., Zhu, H. H., Zhang, C. X., Zhang, W. "Modelling strip footings on slopes using the material point method", Bulletin of Engineering Geology and the Environment, 82(4), 99, 2023. https://doi.org/10.1007/s10064-023-03124-4

[24] Xie, Y., Leshchinsky, B. "Ultimate bearing capacity near slopes: transition from a bearing capacity problem to a slope stability problem", In: Geotechnical Frontiers 2017, Proceedings, 2017, pp. 255–263. https://doi.org/10.1061/9780784480458.025

[25] Zhu, H. H., Wang, Z. Y., Shi, B., Wong, J. K. W. "Feasibility study of strain-based stability evaluation of locally loaded slopes: Insights from physical and numerical modeling", Engineering Geology, 208, pp. 39–50, 2016. https://doi.org/10.1016/j.enggeo.2016.04.019

[26] Baah-Frempong, E., Shukla, S. K. "Stability analysis and design charts for a sandy soil slope supporting an embedded strip footing", International Journal of Geo-Engineering, 9(1), 13, 2018. https://doi.org/10.1186/s40703-018-0082-2

[27] Wang, J. C., Zhu, H. H., Shi, B., Garg, A. "Strain-based stability analysis of locally loaded slopes under variable conditions", Geomechanics and Engineering, 23(3), pp. 289–300, 2020. https://doi.org/10.12989/gae.2020.23.3.289

[28] Zhang, H., Li, C., Chen, W., Xie, N., Wang, G., Yao, W., Jiang, X., Long, J. "Upper-bound limit analysis of the multi-layer slope stability and failure mode based on generalized horizontal slice method", Journal of Earth Science, 35(3), pp. 929–940, 2024. https://doi.org/10.1007/s12583-022-1626-0

[29] Ishak, A. S. A., Jelani, J., Wong, S. Y., Suif, Z., Mazuki, A. L. A. "Stability analysis of a silica sand slope model subjected to surcharge load using LEM and FEM methods", GEOMATE Journal, 27(121), pp. 128–135. 2024.

[30] Zhang, Y., Zhang, F., Yi, Q., Jiang, G., Xie, J. "Material point method-based simulation of run-out characteristics for a soil–rock mixed landslide induced by surcharge", Advances in Civil Engineering, 6255431, 2024. https://doi.org/10.1155/2024/6255431

[31] Rocscience Inc., 2016. SLIDE Version 6.0 – 2D Limit equilibrium slope stability analysis. Rocscience Inc., Toronto, Canada.

[32] Taylor, D. W. "Stability of earth slopes", Boston Society of Civil Engineering, 24(3), pp. 197–247, 1937.

[33] Michalowski, R. L. "Stability charts for uniform slopes", Journal of Geotechnical and Geoenvironmental Engineering, 128(4), pp. 351–355, 2002. https://doi.org/10.1061/(ASCE)1090-0241(2002)128:4(351)

[34] Sun, J. P., Zhao, Z. Y. "Stability charts for homogenous soil slopes", Journal of Geotechnical and Geoenvironmental Engineering, 139(12), pp. 2212–2218, 2013. https://doi.org/10.1061/(ASCE)GT.1943-5606.0000938

[35] Tang, G. P., Zhao, L. H., Li, L., Yang, F. "Stability charts of slopes under typical conditions developed by upper bound limit analysis", Computers and Geotechnics, 65(4), pp. 233–240, 2015. https://doi.org/10.1016/j.compgeo.2014.12.008

[36] Optum Computational Engineering "OptumG2", [computer program] Available at: https://www.optumce.com